



1 **Quantifying the effect of aerosol on vertical velocity and effective terminal**
2 **velocity in warm convective clouds**

3 **Guy Dagan, Ilan Koren*, and Orit Altaratz**

4 Department of Earth and Planetary Sciences, The Weizmann Institute of Science,
5 Rehovot 76100, Israel

6 *Corresponding author. E-mail: ilan.koren@weizmann.ac.il

7

8

9

10 **Abstract**

11 Better representation of cloud–aerosol interactions is crucial for an improved
12 understanding of natural and anthropogenic effects on climate. Recent studies have
13 shown that the overall effect can be viewed as a competition between processes with
14 opposing trends. Here, we reduce the system’s dimensions to its center of gravity
15 (COG), enabling distillation and simplification of the overall trend and its temporal
16 evolution. Within the COG framework, we show that the aerosol effects are nicely
17 reflected by the interplay of the system’s characteristic vertical velocities, namely the
18 updraft (w) and the effective terminal velocity (η). The system’s vertical velocities can
19 be regarded as a sensitive measure for the evolution of the overall trends with time.
20 Using bin-microphysics cloud-scale model, we analyze and follow the trends of the
21 aerosol effect on the magnitude and timing of w and η , and therefore the overall
22 vertical COG velocity. Large eddy simulation model runs are used to upscale the
23 analyzed trends to the cloud-field scale and study how the aerosol effects on temporal
24 evolution of the field’s thermodynamic properties are reflected by the interplay
25 between the two velocities. Our results suggest that aerosol effects on air vertical
26 motion and droplet mobility imply an effect on the way in which water is distributed
27 along the atmospheric column. Moreover, the interplay between w and η predicts the
28 overall trend of the field’s thermodynamic instability. These factors have an important
29 effect on the local energy balance.

30



31 **1. Introduction**

32 Clouds are key players in the Earth's climate system via their influence on the energy
33 balance (Baker and Peter, 2008; Trenberth et al., 2009) and hydrological cycle. Of all
34 of the anthropogenic effects on climate, aerosol's effect on clouds remains one of the
35 most uncertain (Boucher et al., 2013). In warm clouds, aerosol act as cloud
36 condensation nuclei (CCN) around which droplets can form, and therefore aerosol
37 amount and properties determine the initial number of droplets and their size
38 distribution (Squires, 1958; Rosenfeld and Lensky, 1998; Andreae et al., 2004; Koren et
39 al., 2005). The initial droplet concentration affects cloud dynamics via microphysical
40 and dynamical feedback throughout their lifetime. For example, the onset of
41 significant collision events between droplets in polluted clouds (which are initially
42 smaller and more numerous than in clean clouds (Squires, 1958)) is delayed (Gunn
43 and Phillips, 1957; Rosenfeld, 1999, 2000; Squires, 1958; Warner, 1968). This delay
44 can have opposing effects on cloud development by increasing both the water loading
45 (which reduces cloud buoyancy and vertical development) and the latent heat release
46 resulting from the longer and more efficient condensation (increasing cloud buoyancy
47 and vertical development) (Dagan et al., 2015a; Dagan et al., 2015b; Pinsky et al.,
48 2013; Koren et al., 2014). We note that often, these opposing effects act at different
49 stages of the cloud's lifetime, further complicating the prediction of overall trends.

50 Vertical velocities (w) are among the key processes driving convective clouds. The
51 intensity, duration and characteristic size of the updrafts determine the convective
52 clouds' properties. In addition, the clouds' vertical velocity affects the distribution of
53 water along the atmospheric column, thereby having a strong effect on radiation
54 (Koren et al., 2010) and heat balance (Khain et al., 2005). Although previous studies
55 have focused on deep convective clouds, these effects are expected to be significant in
56 warm convective clouds as well. Moreover, warm processes serve as the initial and
57 boundary conditions for mixed-phase processes in deep convective clouds, and
58 therefore gaining a better process understanding of the warm phase is essential for
59 understanding the deeper systems (Chen et al., 2017).

60 The system has another characteristic velocity that measures droplet mobility. This
61 velocity, defined as the effective terminal velocity (η), measures the weighted-by-
62 mass terminal velocity of all hydrometeors within a given volume and therefore



63 defines the falling velocity of the volume's center of gravity (COG) (Koren et al.,
64 2009;Koren et al., 2015) compared to the air vertical velocity. Smaller droplets imply
65 smaller $|\eta|$ (higher mobility) and therefore less deviation from the surrounding air
66 movement. Since η is always negative, smaller $|\eta|$ implies that per a given air updraft,
67 the collective liquid water mass will be carried up higher in the atmosphere. The
68 movement of the COG compared to the surface, defined as V_{COG} , is the vector sum of
69 the two velocities: $V_{\text{COG}} = w - |\eta|$.

70 V_{COG} has recently been shown to be a good measure for the temporal evolution of
71 thermodynamic instability in cloud fields (Dagan et al., 2016). V_{COG} represents the
72 vertical movement of liquid water, which is downward gradient of the net
73 condensation-less-evaporation profile. A negative V_{COG} implies net transport of the
74 liquid water from the cloudy layer to the sub-cloud layer. This holds true for clean
75 precipitation conditions (Dagan et al., 2016), in which the water that condenses in the
76 cloudy layer sediments down to the sub-cloud layer where it partially evaporates. The
77 net condensation in the cloudy layer and the net evaporation in the sub-cloud layer
78 produce a decrease in the thermodynamic instability with time. On the other hand, for
79 the polluted non-precipitating cases, V_{COG} is positive, indicating that the net liquid
80 water movement is upward. The water that is being condensed in the lower part of the
81 cloudy layer is transported upward and evaporates in the upper cloudy and inversion
82 layers (Dagan et al., 2016). The end result of this vertical condensation–evaporation
83 profile is an increase in thermodynamic instability with time.

84 Khain et al. (2005) used a two-dimensional cloud model with spectral (bin)
85 microphysics to study the aerosol effect on deep convective cloud dynamics. They
86 concluded that one of the reasons for comparatively low w in clean maritime
87 convective clouds compared to polluted continental ones is the rapid creation of
88 raindrops. This increases the liquid water loading in the lower part of the cloud,
89 thereby reducing buoyancy. They also claimed that the delayed raindrop production in
90 the continental cloud increases the duration of the diffusion droplet growth stage,
91 which in turn, increases the latent heat release by condensation.

92 Seigel (2014) showed an increase in w with increasing aerosol loading in the cloud
93 core in numerical simulations of a warm convective cloud field. He also showed a



94 decrease in cloud size under polluted conditions due to increased mixing between the
95 clouds and their dry environment.

96 It has been recently shown (Dagan et al., 2015a;Dagan et al., 2015b;Dagan et al.,
97 2017) that under given environmental conditions, warm convective clouds have an
98 optimal aerosol concentration (N_{op}) with respect to their macrophysical properties
99 (such as total mass and cloud top height) and total rain yield. For concentrations
100 smaller than N_{op} , the cloud can be considered as aerosol-limited (Koren et al.,
101 2014;Reutter et al., 2009), and a positive correlation between the aerosol
102 concentration and cloud properties can be expected. Suppressive processes such as
103 enhanced entrainment and water loading take over when the concentrations are higher
104 than N_{op} and reverse the trend. It has also been shown that the value of N_{op} depends
105 heavily on the environmental conditions (thermodynamic conditions that support
106 deeper clouds would have a larger N_{op}).

107 In this work, a bin-microphysics cloud model and large eddy simulation (LES) of a
108 cloud field were used to explore how changes in aerosol concentration affect w and η ,
109 the interplay between them and, as a result, the height of the COG in warm convective
110 clouds (Koren et al., 2009;Grabowski et al., 2006).

111

112 **2. Methodology**

113 **2.1 Single-cloud model**

114 The Tel Aviv University axisymmetric nonhydrostatic cloud model (TAU-CM) with
115 detailed treatment of cloud microphysics (Reisin et al., 1996;Tzivion et al., 1994) was
116 used. The included warm microphysical processes were nucleation of droplets,
117 condensation and evaporation, collision–coalescence, breakup, and sedimentation.
118 The microphysical processes were formulated and solved using a two-moment bin
119 method (Tzivion et al., 1987).

120 The background aerosol size distribution used here represents a clean maritime
121 environment (Jaenicke, 1988). The aerosols are assumed to be composed of NaCl.
122 The different aerosol concentrations (25, 500 and 10,000 cm⁻³, denoted hereafter as
123 25CCN, 500CCN and 10000CCN, respectively) and size distributions are identical to



those used in Dagan et al. (2015a). To study the involved processes, we used a wide range of aerosol loading conditions, from extremely pristine to extremely polluted. To avoid giant CCN effects, the aerosol size distribution was cut at 1 μm (Feingold et al., 1999; Yin et al., 2000; Dagan et al., 2015b).

The model resolution was set to 50 m, in both the vertical and horizontal directions, and the time step to 1 s. The initial conditions were based on theoretical atmospheric profiles that describe a tropical environment (Malkus, 1958) (see profile T1RH2 in Fig. 1 in Dagan et al., 2015a). They consisted of a well-mixed sub-cloud layer between 0 and 1000 m, a conditionally unstable cloudy layer (6.5°C/km) between 1000 and 4000 m, and an overlying inversion layer (temperature gradient of 2°C over 50 m). The relative humidity (RH) in the cloudy (inversion) layer was 90% (30%). The results presented here were examined for a few different sets of initial conditions (different inversion-base heights and RH in the cloudy layer—analysis not shown). The general conclusions were found to be insensitive to the initial conditions.

To examine the effect of aerosols on the entire cloud, the properties presented in this work are cloud mean values weighted by the liquid water mass in each grid cell. Cloudy grid cells were defined as cells with liquid water content larger than 0.01 g/kg. The cloud's COG (Koren et al., 2009; Grabowski et al., 2006) was calculated as:

$$COG = \frac{\sum m_i z_i}{\sum m_i} \quad (1)$$

where m_i and z_i are the mass [kg] and height [m] of voxel i , respectively.

The η (effective terminal velocity) was calculated according to Koren et al. (2015):

$$\eta = \frac{\sum V_{t_j} m_j n_j}{\sum m_j n_j} \quad (2)$$

where V_{t_j} , m_j and n_j are the terminal velocity [m/s], mass [kg] and concentration [cm^{-3}] of droplets in bin j , respectively. This was calculated for all cloudy grid cells.



151 **2.2 LES**

152 We used the System for Atmospheric Modeling (SAM) LES model (Khairoutdinov
 153 and Randall, 2003) with a bin-microphysics scheme (Khain and Pokrovsky, 2004) to
 154 simulate the BOMEX (Barbados Oceanographic and Meteorological EXperiment)
 155 warm cumulus case study (Holland and Rasmusson, 1973; Siebesma et al., 2003). The
 156 horizontal resolution was set to 100 m, the vertical resolution to 40 m. The domain
 157 size was $12.8 \times 12.8 \times 4.0 \text{ km}^3$ and the time step was 1 s. We ran the model for 16 h,
 158 but the statistical analysis included only the last 14 h of the simulation. We used 8
 159 different aerosol concentrations: 5, 25, 50, 100, 250, 500, 2000 and 5000 cm^{-3} . Again,
 160 we used a marine background aerosol size distribution (Jaenicke, 1988). Further
 161 details about the simulations can be found in Dagan et al. (2017).

162

163 **3. Results and discussion**

164 **3.1 Single cloud: vertical velocity and effective terminal velocity**

165 Starting from the single-cloud scale, we first followed mean w , mean η , mean V_{COG} ,
 166 and COG height as a function of time for the three different levels of aerosol loading
 167 ($25, 500, \text{ and } 10,000 \text{ cm}^{-3}$). From an early stage of the cloud's evolution, the cleanest
 168 cloud (25CCN) had the lowest COG. This was a result of the lower w (Fig. 1a) and
 169 larger absolute value of the negative η (caused by the initially larger droplets – Fig.
 170 1b), which together cause a lower V_{COG} (Fig. 1c). At the early stages of the polluted
 171 clouds, the 500CCN and 10000CCN COG moved upward at the same rate. After
 172 about 60 min of simulation, the 500CCN's COG started to decrease while the
 173 10000CCN's COG remained relatively high. This trend could not be explained by the
 174 cloud's mean w (Fig. 1a). The 500CCN's w was higher than that of the 10000CCN
 175 during the period between 50 and 63 min of simulation. Without considering the
 176 effect of η on the COG, one would expect that the 500CCN's COG would be higher
 177 than that of the 10000CCN. The 500CCN had lower (more negative) values of η than
 178 the 10000CCN, which decreased the height of its COG compared to the 10000CCN.
 179 These larger negative values of η in the 500CCN were due to the rain that developed
 180 from this cloud (the rain from the 10000CCN is negligible), which led to lower
 181 mobility (lower ability to move with the ambient air (Koren et al., 2015)).



Figure 1 demonstrates the importance of the aerosol effect on both w and η in determining the COG height. Figure 2 presents the evolution of the clouds on the phase space span by w vs. V_{COG} . All clouds began their evolution on the 1:1 line. This means that at the early stages of the cloud's evolution, $\eta \sim 0$ and hence $V_{\text{COG}} \sim w$. After about 40 min of simulation, the cleanest cloud's (25CCN) trajectory began to deviate from the 1:1 line to the left, demonstrating an increase in $|\eta|$ and hence lower droplet mobility. The deviation from the 1:1 line occurred later (at about $t = 55$ min of simulation) in the more polluted simulation (500CCN), whereas for the most polluted clouds (10000CCN), the lack of significant collision-coalescence and rain production resulted in evolution on the 1:1 line throughout the cloud's lifetime. This delay in the deviation from the 1:1 line (increasing the time for which $\eta \sim 0$) demonstrates the increase in droplet mobility with aerosol loading. The longer period for which $\eta \sim 0$ in the polluted cases enables the water mass to be pushed higher into the atmosphere and hence (together with the increase in the air vertical velocity – Fig. 1a) to produce cloud invigoration by the aerosol (Koren et al., 2015).

197

198 **3.2 LES results: aerosol effect on the vertical velocity and effective terminal** 199 **velocity in cloud fields**

Shifting our view from the single-cloud scale to the cloud-field scale adds another layer of complexity as clouds affect the way in which the whole field's thermodynamics evolve with time. Aerosol concentration has recently been shown to determine the trend of this evolution (Dagan et al., 2016; Dagan et al., 2017). Clean precipitating clouds act to consume the initial instability that created them by warming the cloudy layer (in which there is net condensation) and cooling the sub-cloud layer (by rain evaporation). On the other hand, polluted non-precipitating clouds act to increase the field's instability by cooling and moistening the upper cloudy and inversion layers.

Figure 3 presents the domain's mean w (in both space and time, weighted by the liquid water mass to be consistent with the COG view) vs. the domain mean η . The color-coding in Fig. 3 denotes the different aerosol concentrations. In agreement with previous studies (Saleeby et al., 2015; Seigel, 2014), an increase in aerosol loading yielded an increase in w . This increase is driven by larger latent heat contribution to



the cloud's buoyancy due to the increased condensation efficiency (Dagan et al., 2015a; Dagan et al., 2017; Koren et al., 2014; Pinsky et al., 2013; Seiki and Nakajima, 2014) and thermodynamic instability (Dagan et al., 2016; Dagan et al., 2017). In parallel, aerosol shifts to smaller droplets (Squires, 1958) and reduces the magnitude of η , indicating better mobility of the smaller droplets (Koren et al., 2015). The outcome of these two effects (that work together to push the water mass higher in the atmosphere) is an increase in COG height with aerosol loading (Heiblum et al., 2016b; Dagan et al., 2017).

In the single-cloud-scale analysis (section 3.1), we showed how the timing of the evolution of the two velocities dictates the aerosol effect. Here, having many clouds in the field in different stages of their lifetimes, we first analyzed the bulk properties of the two velocities. With the intention of quantifying the relative contribution of the aerosol effect on the mean COG height by modulating w and η , we plotted them one against the other for all of the simulations that differed in aerosol loading and for all clouds in the domain (Fig. 3a). For the entire simulation period, the η vs. w scatter plot resulted in an almost a straight line ($R^2 = 0.96$) which was sorted by aerosol concentration with a slope of 0.69. This means that an increase in aerosol concentration that will result in a 1 m/s increase in mean w will drive a decrease in the magnitude of η by 0.69 m/s. In other words, the relative contribution to the changes in the mean COG height in the domain caused by the increase in aerosol loading (Heiblum et al., 2016b; Dagan et al., 2017) during the entire simulation is ~60% due to changes in w and ~40% due to changes in η .

To include the aerosol effect on the cloud-field-scale thermodynamic properties, we divided the simulation periods into three equal thirds (excluding the first 2 h, each third of a period covered 4 h and 40 min). The x and * markers in Fig. 3a represent the first third (2 h to 6 h 40 min into the simulation) and last third (11 h 20 min to 16 h into the simulation), respectively. During the first third, the slope of w vs. η was steeper than the mean over the entire simulation (slope of 0.92 with $R^2 = 0.96$); during the last third, it was more gradual (slope of 0.47 with $R^2 = 0.87$). The almost 1:1 relation between w and η in the first third of the simulation period suggests a comparable contribution in determining the aerosol effect on mean COG height. However, the relative contribution of η decreases as the simulation progresses, to about 1/3 during the last third of the simulation period (compared with 2/3 of w).



247 The decrease in the w vs. η slopes toward the end of the simulations is driven by the
 248 changes in the thermodynamic instability. The increase in instability under polluted
 249 conditions produces an increase in mean w (Dagan et al., 2016). Nevertheless,
 250 increased instability and deepening of the cloud layer are not sufficient to produce a
 251 significant amount of rain under the most polluted simulations and hence, there is no
 252 increase in the magnitude of η . An increase in w with no change in η is manifested as
 253 a horizontal shift to the right on the η vs. w phase space (red arrow in Fig. 3a). On the
 254 other hand, the decreased instability under clean conditions produces a decrease in
 255 both mean w and the rain amount (Dagan et al., 2017), and therefore in $|\eta|$ (blue arrow
 256 in Fig. 3a). The end result of the different changes in w and η under clean and polluted
 257 conditions is a decrease in the slope of η vs. w and therefore, a decrease in the relative
 258 contribution of η to the aerosol effect on the mean COG.

259

260 In Fig. 3a, the presented quantities are domain and time averages. Figure 1 showed
 261 that the relative contribution of w and η to the aerosol effect on COG height strongly
 262 depends on the stage of the cloud's evolution. The averaging in Fig. 3a mixes many
 263 clouds at different stages in their evolution and represents the effect on the mean COG
 264 in the domain. To further explore the relative contribution of the aerosol effect on w
 265 and η as a function of cloud-evolution stage, we used a cloud-tracking algorithm
 266 (Heiblum et al., 2016a). We identified the growing stage of the clouds as the stage for
 267 which the cloud top ascends. Figure 3b presents the η vs. w phase space only for
 268 clouds in their growing stage. Table 1 presents the slopes of the linear regression lines
 269 for the entire simulation time and for the different thirds of the simulation period. The
 270 decrease with time in the relative contribution of η compared to w to the aerosol effect
 271 on COG height was also seen for the growing clouds (see the decrease in the slope
 272 with time). This, again, was due to the changes in thermodynamic conditions.

273 As shown for the cloud scale, one of the most notable aerosol effects can be viewed as
 274 delaying the onset of significant collection processes in the polluted clouds (Koren et
 275 al., 2015), and therefore delaying the increase in η values early in the cloud's lifetime.
 276 Therefore, during the growing stage, the relative contribution of η was higher (Fig.
 277 3b) as compared to "all clouds" (Fig. 3a). This was demonstrated by the increasing
 278 slope of the η vs. w phase space during the growing stage (Table 1).



279

280 To quantify the evolution of the thermodynamic instability with time as a function of
281 aerosol loading, we looked at the time trends in the η vs. w phase space. We defined
282 the angle ‘ A ’ as the angle between the time trend points on the η vs. w phase space per
283 given aerosol loading (the line that connects the first and last thirds of the simulation
284 and the x-axis on the η vs. w —see schematic definition of A in Fig. 3b). We note that
285 A rotates counter-clockwise with increasing aerosol loading (Fig. 3a). It starts as
286 $\sim 100^\circ$ for the cleanest simulation and monotonically increases with aerosol loading to
287 $\sim 360^\circ$ for the most polluted simulations (Fig. 4b). A between 90° and 180° (as shown
288 for clean cases—Fig. 4b) represents a decrease in both w and $|\eta|$ and hence a decrease
289 in the thermodynamic instability with time. A between 270° and 360° , on the other
290 hand (as shown for the most polluted cases—Fig. 4b), represents an increase in both w
291 and $|\eta|$ and hence an increase in the thermodynamic instability with time.

292 The sign of V_{COG} has been shown to predict the evolution of thermodynamic
293 instability (Dagan et al., 2016). Thus, correlations between A and V_{COG} are expected.
294 Figure 4 presents V_{COG} (Fig. 4a) and A (Fig. 4b) as a function of the aerosol loading,
295 and V_{COG} vs. A (Fig. 4c). Figure 4a and b demonstrates that both the V_{COG} and A
296 increase monotonically with aerosol loading following a similar trend. V_{COG} and A
297 cross the 0 and 180° lines, respectively, at similar aerosol concentrations, representing
298 the transition between consumption and production of the thermodynamic instability
299 (Dagan et al., 2016). Figure 4c further demonstrates an almost perfect linear
300 correlation ($R^2 = 0.99$) between V_{COG} and A sorted by aerosol concentration.

301

302 **3.3 Summary**

303 Clouds form a complex system in which microphysical and dynamical processes are
304 tightly linked and modulated by the thermodynamic properties of the environment. In
305 turn, on the cloud-field scale, clouds affect the field’s thermodynamic conditions. The
306 aerosol effect on droplet size distribution therefore affects all of the above.

307 Analyzing the two characteristic velocities on the cloud scale allows separation, as a
308 first approximation, between the aerosol effects on condensation/evaporation
309 efficiencies (reflected by the magnitude of w) and those on droplet mobility (reflected



310 by the inverse magnitude of η). The magnitudes of w and η act in opposite ways, i.e.,
 311 stronger w and smaller $|\eta|$ imply more efficient transport of liquid water to the upper
 312 atmosphere. We use their sum, defined as V_{COG} , to estimate the overall effect on the
 313 COG's vertical movement. Single-cloud analysis showed the timing of this interplay
 314 and how each velocity affects the COG elevation. It showed that the invigorating
 315 aerosol effect can be viewed mostly at the early stages of cloud development, when an
 316 increase in aerosol loading enhances the condensation efficiency (reflected as higher
 317 w levels) and delays the onset of significant collection processes (reflected as a delay
 318 in the sharp increase in η). Both act to transfer liquid water higher into the atmosphere
 319 (Koren et al., 2015). Later, as the cloud dissipates, the “payment” is viewed as
 320 enhanced evaporation, and if the cloud manages to reach the significant collection-
 321 process stage, then the surface rain is stronger (expressed as a sharp increase in $|\eta|$).

322 Similar to the single-cloud case, the LES results demonstrated an increase in w and
 323 decrease in the magnitude of η (less negative η) with aerosol loading, both yielding a
 324 higher COG. We analyzed the bulk properties of the two velocities for the entire
 325 simulation time (14 h) and for all clouds in the domain and showed that the relative
 326 contribution of the aerosol effect on w and η in determining COG evolution is
 327 comparable (60% and 40%, respectively). However, at the beginning of the
 328 simulation, this ratio was almost 1:1, and the relative contribution of η decreased with
 329 time. Such temporal changes in the w vs. η slope indicate changes in the
 330 thermodynamic properties of the field (Dagan et al., 2016). Increasing thermodynamic
 331 instability under polluted conditions results in an increase in mean w , while the
 332 decreasing instability under clean condition results in a decrease in rain amount and
 333 hence, in η . Both trends act to reduce the slope.

334 Using a cloud-tracking algorithm, we identified the growing stage of the clouds and
 335 examined the relative contribution of the aerosol effect on COG height by modulating
 336 w and η during this stage. We showed that the relative contribution of the aerosol
 337 effect on η is larger during the growing stage (for which aerosol loading acts to
 338 maintain lower $|\eta|$ for a longer time) compared to the mature and dissipating stages,
 339 thereby strengthening the argument that most of the aerosol invigoration effect occurs
 340 early in the cloud's evolution (Koren et al., 2015).

341



342 *Data availability.* Information about the model and initialization files are available
343 upon request to the contact author.

344

345 *Competing interests.* The authors declare that they have no conflict of interest.

346 **References**

347

348 Andreae, M. O., Rosenfeld, D., Artaxo, P., Costa, A. A., Frank, G. P., Longo, K. M.,
349 and Silva-Dias, M. A. F.: Smoking rain clouds over the Amazon, Science,
350 303, 1337-1342, 10.1126/science.1092779, 2004.

351 Baker, M. B., and Peter, T.: Small-scale cloud processes and climate, Nature, 451,
352 299-300, 10.1038/nature06594, 2008.

353 Boucher, O., Randall, D., Artaxo, P., Bretherton, C., Feingold, G., Forster, P.,
354 Kerminen, V., Kondo, Y., Liao, H., and Lohmann, U.: Clouds and aerosols,
355 Climate Change, 571-657, 2013.

356 Chen, Q., Koren, I., Altaratz, O., Heiblum, R. H., Dagan, G., and Pinto, L.: How do
357 changes in warm-phase microphysics affect deep convective clouds?,
358 Atmospheric Chemistry and Physics, 17, 9585-9598, 2017.

359 Dagan, G., Koren, I., and Altaratz, O.: Competition between core and periphery-based
360 processes in warm convective clouds—from invigoration to suppression,
361 Atmospheric Chemistry and Physics, 15, 2749-2760, 2015a.

362 Dagan, G., Koren, I., and Altaratz, O.: Aerosol effects on the timing of warm rain
363 processes, Geophysical Research Letters, 42, 4590-4598,
364 10.1002/2015GL063839, 2015b.

365 Dagan, G., Koren, I., Altaratz, O., and Heiblum, R. H.: Aerosol effect on the
366 evolution of the thermodynamic properties of warm convective cloud fields,
367 Scientific Reports, 6, 38769, 2016.

368 Dagan, G., Koren, I., Altaratz, O., and Heiblum, R. H.: Time-dependent, non-
369 monotonic response of warm convective cloud fields to changes in aerosol
370 loading, Atmos. Chem. Phys., 17, 7435-7444, 10.5194/acp-17-7435-2017,
371 2017.

372 Feingold, G., Cotton, W. R., Kreidenweis, S. M., and Davis, J. T.: The impact of giant
373 cloud condensation nuclei on drizzle formation in stratocumulus: Implications
374 for cloud radiative properties, Journal of the Atmospheric Sciences, 56, 4100-
375 4117, 10.1175/1520-0469(1999)056<4100:tiogcc>2.0.co;2, 1999.

376 Grabowski, W., Bechtold, P., Cheng, A., Forbes, R., Halliwell, C., Khairoutdinov, M.,
377 Lang, S., Nasuno, T., Petch, J., and Tao, W. K.: Daytime convective
378 development over land: A model intercomparison based on LBA observations,
379 Quarterly Journal of the Royal Meteorological Society, 132, 317-344, 2006.

380 Gunn, R., and Phillips, B.: An experimental investigation of the effect of air pollution
381 on the initiation of rain, Journal of Meteorology, 14, 272-280, 1957.

382 Heiblum, R. H., Altaratz, O., Koren, I., Feingold, G., Kostinski, A. B., Khain, A. P.,
383 Ovchinnikov, M., Fredj, E., Dagan, G., and Pinto, L.: Characterization of
384 cumulus cloud fields using trajectories in the center of gravity versus water
385 mass phase space: 1. Cloud tracking and phase space description, Journal of
386 Geophysical Research: Atmospheres, 2016a.



- 387 Heiblum, R. H., Altaratz, O., Koren, I., Feingold, G., Kostinski, A. B., Khain, A. P.,
388 Ovchinnikov, M., Fredj, E., Dagan, G., and Pinto, L.: Characterization of
389 cumulus cloud fields using trajectories in the center-of-gravity vs. water mass
390 phase space. Part II: Aerosol effects on warm convective clouds, *Journal of*
391 *Geophysical Research: Atmospheres*, 2016b.
- 392 Holland, J. Z., and Rasmusson, E. M.: Measurements of the atmospheric mass,
393 energy, and momentum budgets over a 500-kilometer square of tropical ocean,
394 *Monthly Weather Review*, 101, 44-55, 1973.
- 395 Jaenicke, R.: Aerosol physics and chemistry, *Landolt-Börnstein Neue Serie*, 4b, 391–
396 457, 1988.
- 397 Khain, A., and Pokrovsky, A.: Simulation of effects of atmospheric aerosols on deep
398 turbulent convective clouds using a spectral microphysics mixed-phase
399 cumulus cloud model. Part II: Sensitivity study, *Journal of the Atmospheric*
400 *Sciences*, 61, 2983-3001, 10.1175/jas-3281.1, 2004.
- 401 Khain, A., Rosenfeld, D., and Pokrovsky, A.: Aerosol impact on the dynamics and
402 microphysics of deep convective clouds, *Quarterly Journal of the Royal*
403 *Meteorological Society*, 131, 2639-2663, 10.1256/qj.04.62, 2005.
- 404 Khairoutdinov, M. F., and Randall, D. A.: Cloud resolving modeling of the ARM
405 summer 1997 IOP: Model formulation, results, uncertainties, and sensitivities,
406 *Journal of the Atmospheric Sciences*, 60, 2003.
- 407 Koren, I., Kaufman, Y. J., Rosenfeld, D., Remer, L. A., and Rudich, Y.: Aerosol
408 invigoration and restructuring of Atlantic convective clouds, *Geophysical*
409 *Research Letters*, 32, 10.1029/2005gl023187, 2005.
- 410 Koren, I., Altaratz, O., Feingold, G., Levin, Z., and Reisin, T.: Cloud's Center of
411 Gravity - a compact approach to analyze convective cloud development,
412 *Atmospheric Chemistry and Physics*, 9, 155-161, 2009.
- 413 Koren, I., Remer, L. A., Altaratz, O., Martins, J. V., and Davidi, A.: Aerosol-induced
414 changes of convective cloud anvils produce strong climate warming,
415 *Atmospheric Chemistry and Physics*, 10, 5001-5010, 10.5194/acp-10-5001-
416 2010, 2010.
- 417 Koren, I., Dagan, G., and Altaratz, O.: From aerosol-limited to invigoration of warm
418 convective clouds, *science*, 344, 1143-1146, 2014.
- 419 Koren, I., Altaratz, O., and Dagan, G.: Aerosol effect on the mobility of cloud
420 droplets, *Environmental Research Letters*, 10, 104011, 2015.
- 421 Malkus, J. S.: On the structure of the trade wind moist layer, 1958.
- 422 Pinsky, M., Mazin, I., Korolev, A., and Khain, A.: Supersaturation and diffusional
423 droplet growth in liquid clouds, *Journal of the Atmospheric Sciences*, 70,
424 2778-2793, 2013.
- 425 Reisin, T., Levin, Z., and Tzivion, S.: Rain Production in Convective Clouds As
426 Simulated in an Axisymmetric Model with Detailed Microphysics. Part I:
427 Description of the Model, *Journal of the Atmospheric Sciences*, 53, 497-519,
428 10.1175/1520-0469(1996)053<0497:RPICCA>2.0.CO;2, 1996.
- 429 Reutter, P., Su, H., Trentmann, J., Simmel, M., Rose, D., Gunthe, S., Wernli, H.,
430 Andreae, M., and Pöschl, U.: Aerosol-and updraft-limited regimes of cloud
431 droplet formation: influence of particle number, size and hygroscopicity on the
432 activation of cloud condensation nuclei (CCN), *Atmospheric Chemistry and*
433 *Physics*, 9, 7067-7080, 2009.
- 434 Rosenfeld, D., and Lensky, I. M.: Satellite-based insights into precipitation formation
435 processes in continental and maritime convective clouds, *Bulletin of the*



- 436 American Meteorological Society, 79, 2457-2476, 10.1175/1520-
437 0477(1998)079<2457:sbiipf>2.0.co;2, 1998.
- 438 Rosenfeld, D.: TRMM observed first direct evidence of smoke from forest fires
439 inhibiting rainfall, *Geophysical Research Letters*, 26, 3105-3108,
440 10.1029/1999gl006066, 1999.
- 441 Rosenfeld, D.: Suppression of rain and snow by urban and industrial air pollution,
442 *Science*, 287, 1793-1796, 10.1126/science.287.5459.1793, 2000.
- 443 Saleeby, S. M., Herbener, S. R., van den Heever, S. C., and L'Ecuyer, T.: Impacts of
444 Cloud Droplet–Nucleating Aerosols on Shallow Tropical Convection, *Journal*
445 *of the Atmospheric Sciences*, 72, 1369-1385, 2015.
- 446 Seigel, R. B.: Shallow Cumulus Mixing and Subcloud Layer Responses to Variations
447 in Aerosol Loading, *Journal of the Atmospheric Sciences*, 2014.
- 448 Seiki, T., and Nakajima, T.: Aerosol effects of the condensation process on a
449 convective cloud simulation, *Journal of the Atmospheric Sciences*, 71, 833-
450 853, 2014.
- 451 Siebesma, A. P., Bretherton, C. S., Brown, A., Chlond, A., Cuxart, J., Duynkerke, P.
452 G., Jiang, H., Khairoutdinov, M., Lewellen, D., and Moeng, C. H.: A large
453 eddy simulation intercomparison study of shallow cumulus convection,
454 *Journal of the Atmospheric Sciences*, 60, 1201-1219, 2003.
- 455 Squires, P.: The microstructure and colloidal stability of warm clouds, *Tellus*, 10,
456 262-271, 1958.
- 457 Trenberth, K. E., Fasullo, J. T., and Kiehl, J.: Earth's global energy budget, *Bull.*
458 *Amer. Meteor. Soc.*, 90, 311-323, 2009.
- 459 Tzivion, S., Feingold, G., and Levin, Z.: An efficient numerical solution to the
460 stochastic collection equation, *Journal of the atmospheric sciences*, 44, 3139-
461 3149, 1987.
- 462 Tzivion, S., Reisin, T., and Levin, Z.: Numerical simulation of hygroscopic seeding in
463 a convective cloud, *Journal of Applied Meteorology*, 33, 252-267, 1994.
- 464 Warner, J.: A reduction in rainfall associated with smoke from sugar-cane fires—An
465 inadvertent weather modification?, *Journal of Applied Meteorology*, 7, 247-
466 251, 1968.
- 467 Yin, Y., Levin, Z., Reisin, T. G., and Tzivion, S.: The effects of giant cloud
468 condensation nuclei on the development of precipitation in convective
469 clouds—a numerical study, *Atmospheric research*, 53, 91-116, 2000.

470

471

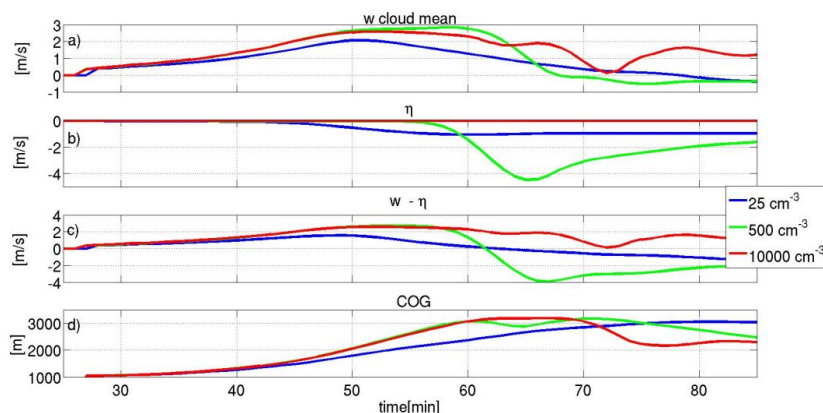


Figure 1. (a) Mean vertical velocity (w), (b) mean effective terminal velocity (η), (c) mean vertical velocity plus effective terminal velocity, and (d) cloud center of gravity (COG) as a function of time for three different aerosol concentrations.

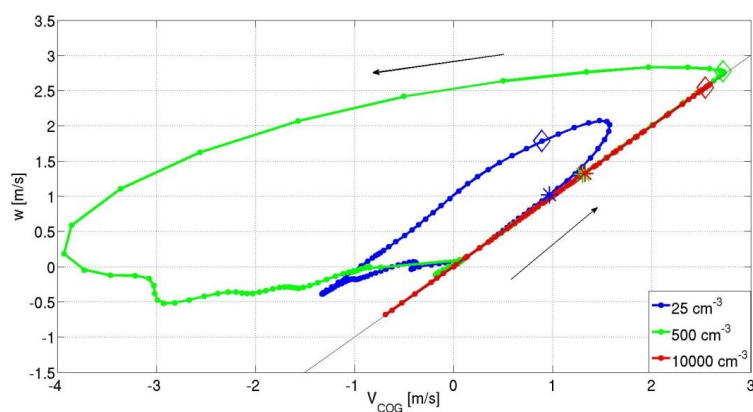
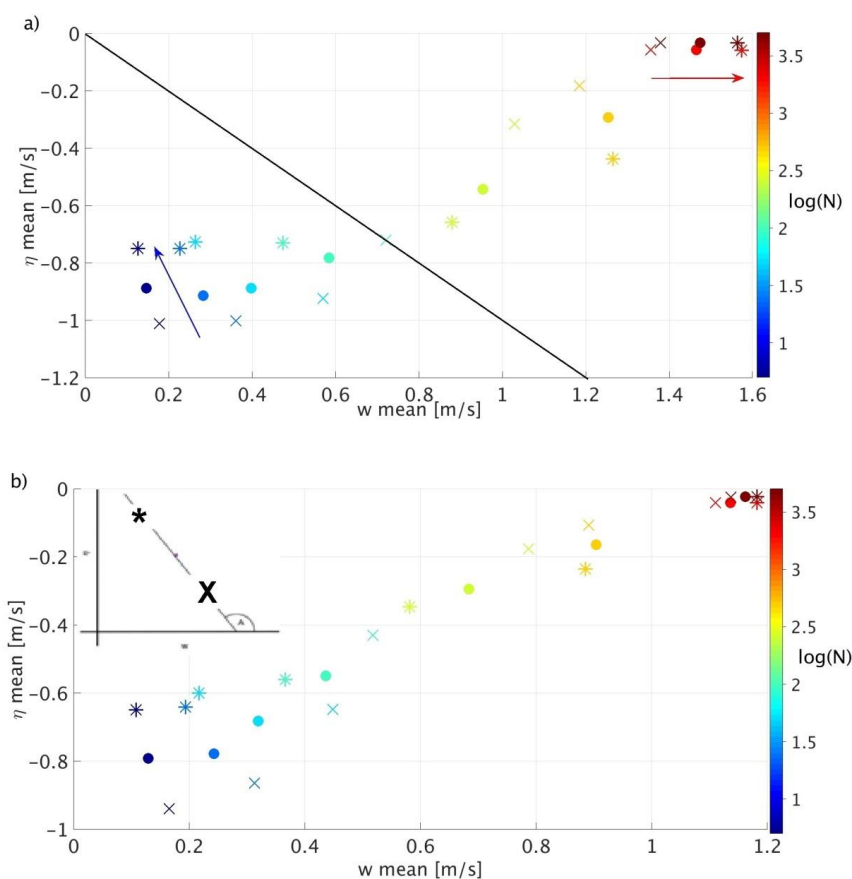


Figure 2. Cloud evolution on the phase space span by w vs. V_{COG} . The arrows mark the direction of the trajectories and the thin black line is the 1:1 line. Stars and diamonds denote $t = 40$ min and 55 min of the simulation, respectively.



482

483 **Figure 3. Temporal and spatial averages of the ambient air vertical velocity (w)**
 484 **vs. effective terminal velocity (η).** Color-coding denotes the different aerosol
 485 **concentrations. Dots represent averages of the entire simulation data (excluding**
 486 **the first 2 h spin-up time). The x and * markers represent the first third (2 h to 6**
 487 **h 40 min) and last third (11 h 20 min to 16 h) of the simulation period,**
 488 **respectively. (a) All clouds in the domain. (b) Only clouds in the growing stage.**
 489 **The black line in (a) is the zero-sum line for which $V_{COG} = 0$ (below the line V_{COG}**
 490 **< 0 and above it $V_{COG} > 0$). The angle A that measures the η vs. w time trend per**
 491 **aerosol level is illustrated in the inset in panel b.**

492



Table 1. Linear regression slope on the η vs. w phase space for the different periods of the simulations for all clouds and growing-stage clouds in the domain. R^2 of the regression lines is presented in parentheses.

	All clouds	Growing clouds
Total simulation period (2–14 h)	0.69 (0.96)	0.79 (0.98)
First period of simulation (2–6:40 h)	0.92 (0.96)	0.99 (0.93)
Last period of simulation (11:20–16 h)	0.47 (0.87)	0.59 (0.98)

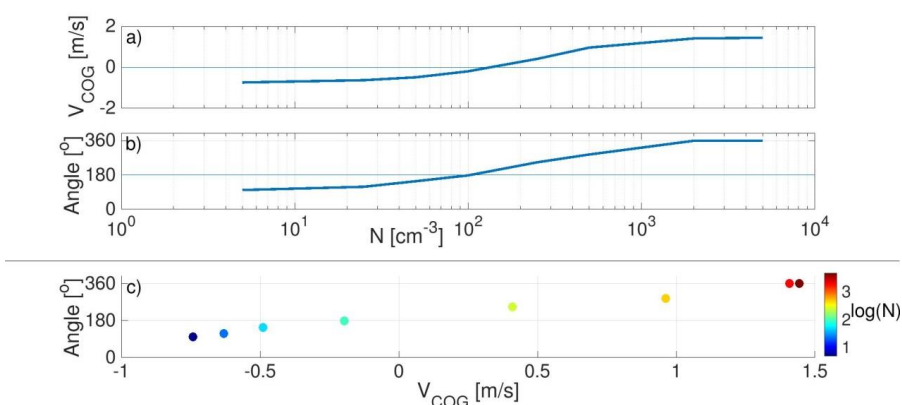


Figure 4. (a) The cloud field's mean value of V_{COG} and (b) the angle A between the line that connect the first and last thirds of the simulation period and the x-axis on the η vs. w phase space for all clouds in the domain (Fig. 3a) as a function of aerosol loading. (c) V_{COG} vs. A . Color-coding denotes the different aerosol concentrations.